Nano World Journal

https://doi.org/10.17756/nwj.2024-s1-003

Research Article

Open Access

Optical Properties of Niobium(V) Oxide Nanoparticles Synthesized by Thermolysis Method

Kavita Mandre[1], Jaiveer Singh[2*], Jitendra Tripathi[2], Netram Kaurav[3] and Puja Singh[4]

[1]*Department of Physics, Government P.G. College Barnagar, Ujjain, Madhya Pradesh,India*
[2]*Department of Physics, ISR, IPS Academy, Indore, Madhya Pradesh, India*
[3]*Department of Physics, Government Holkar Science College, Indore, Madhya Pradesh, India*
[4]*Department of Electronics and Communication Engineering, Medi-Caps University, Indore, Madhya Pradesh, India*

[*]Correspondence to:
Jaiveer Singh
Department of Physics,
ISR, IPS Academy,
Indore, Madhya Pradesh, India.
E-mail: jaiveer24singh@gmail.com

Received: January 03, 2024
Accepted: March 04, 2024
Published: March 07, 2024

Citation: Mandre K, Singh J, Tripathi J, Kaurav N, Singh P. 2024. Optical Properties of Niobium(V) Oxide Nanoparticles Synthesized by Thermolysis Method. *Nano World J* 10(S1): S10-S13.

Published by United Scientific Group

Abstract

Niobium(V) oxide (Nb_2O_5) is an attractive dynamic material for technologies such as catalysis, sensors, energy storage and electrochromic devices because of its peculiar optical, electrical, and electrochemical properties. Here, we report the synthesis of Nb_2O_5 nanoparticles (NPs) by thermal decomposition route by changing the quantity of capping agent polyvinyl pyrrolidone (PVP) and calcination at 700 °C. X-ray diffraction (XRD) and ultraviolet-visible (UV-Vis) spectroscopy in diffuse reflectance mode, Raman spectroscopy and Fourier transform infrared spectroscopy (FTIR) were used to investigate the crystallographic phases, optical, vibronic characteristics and presence of different functional groups, respectively. The average crystallite sizes were calculated by Scherrer's relation, which were found to be ~23 nm and ~18 nm, respectively, for the orthorhombic phase in both sample A and sample B. Raman spectra indicates presence of different stretching and vibrational modes corresponding to NbO_6 octahedra in the samples. FTIR spectra show different bands that clearly indicate stretching and bending vibrations of Nb and O. By analyzing UV-Vis absorption spectra, the value of energy band gaps for sample A and sample B were obtained as 3.22 eV and 3.19 eV.

Keywords

X-ray diffraction, Nanoparticles, Ultraviolet-visible spectroscopy, Raman spectroscopy, Thermal decomposition

Introduction

Nanotechnology involving various types of nanostructures such as thin films, nanotubes, nanoparticles, etc., has grown to be one of the most active fields in adaptable materials science over the past few decades [1, 2]. It has wide range of applications, mostly as a result of the particular size-dependent characteristics. Due to their small size and huge surface area, NPs have drawn a lot of interest. Metal-oxide nanoparticles (MONPs) stand out among these materials as viable contenders in chemistry, materials science, physics, and biology fields [3]. The insulator, semiconductor, and conductor characteristics of nanomaterials are determined by their specific electronic structure, which in turn depends on the valence electrons. In general, transition metal ions have empty d-shells, which enable reactive electronic transitions, large band gaps, excellent electrical properties and high dielectric constants. Because of this, MONPs have outstanding and controllable optoelectronic, photochemical, optical, electrical, thermal, magnetic, catalytic, and mechanical properties. Due to their unusual size and shape, MONPs are also used as fuel cells, sensors, actuators, batteries, optical devices, pyroelectric, piezoelectric, supercapacitors, and ferroelectric devices, as well as random access

memory devices [4]. Semiconducting metal oxide-based gas sensors have also sparked considerable interest due to features such as quick and sensitive detection, mobility and cheap cost as compared to other traditional approaches. Because of their unique features, man-made MONPs are among the most widely used materials [3, 4]. Different oxides play a significant part in the rapidly evolving field of semiconducting device research and among them, oxides of niobium plays an important role in this field. Owing to its importance, this work is focused on niobium oxides. Since niobium is a transition metal with compounds that have different oxidation states like +1, +2, +3, +4, and +5, it is comparable to oxygen, which has an oxidation state of -2. As a result, there are many posiible forms of oxides, including NbO, NbO_2, and Nb_2O_5. Out of these, NbO is utilized as a battery electrode and possesses superconducting qualities. It also has a cubic phase, while NbO_2 contains tetragonal and monoclinic phases, as well as semiconducting-metallic features; nonetheless, it has less electronic conductivity than NbO. Nb_2O_5 is the oxide that is more stable than the other two oxide species. Therefore, in semiconductors, Nb_2O_5 is widely used. It is frequently utilized as an electrode in lithium batteries. By altering its temperature, Nb_2O_5 frequently modifies its structure. As a result, Nb_2O_5 has several phases, including T-phase, TT-B-phase, and others [2]. Nb_2O_5 NPs have excellent ability like high thermal stability, wide range of activity in ultraviolet and infrared region and wider band gap so these are used in optical glasses and are also used in catalyst [5]. Niobium oxides make a complex system with a variety of polymorphic phases. They have unique properties that enable them to take on a variety of forms, allowing them to be applied in science and technology. Another area of active research is the resistive switching characteristic of Nb_2O_5, which could allow the creation of memristors and their application as non-volatile memory devices [6]. These applications and unique properties have motivated us to synthesize Nb_2O_5 NPs using PVP as the capping agent and to characterize their peroperties using various techniques in this work.

Experimentation

Synthesis

In the current study, Nb_2O_5 NPs were synthesized by thermal decomposition method. The synthesized Nb_2O_5 NPs were named as sample A and sample B as per PVP amount of 0.35 g and 0.5 g. For synthesis of sample A. Typically, 0.25 g of niobium(V) chloride (99% purity, Sigma-Aldrich, molar weight = 270.17 g/mol) with 0.35 g of PVP were melted in a flask using 50 ml of pure water, and the combination was stirred thoroughly for 60 min at 90 °C. Here, PVP was used as a capping agent. Further, the obtained product was calcined at 700 °C for 150 min in a typical furnace. The mixture was given treatment before being allowed to reach room temperature. The acquired material was further thoroughly crushed and hand ground to obtain niobium oxide nanoparticles in white powder form. Similar procedures were followed for 0.5 g PVP (Sample B).

XRD measurements

The XRD measurement was performed by an "AXRD powder diffraction system" by "PROTO Manufacturing" using Cu-Kα radiation in the 2θ range from 20° to 80°. The Gaussian function was used to fit the peaks to extract average crystallite size. We have determined the average crystallite size by applying the standard Scherrer's formula (Equation 1).

$$D = \frac{0.9\lambda}{\beta \cos\theta} \quad (1)$$

Where, D = crystalline size, λ = X-ray wavelength, θ = Bragg's angle, β = Full width half maximum.

UV-Vis diffuse reflectance spectroscopy and Raman spectroscopy

UV-Vis spectroscopy was used to determine the energy band gap, while Raman spectroscopy was used to conduct vibrational characterization. UV-Vis measurements were performed by UV-Vis (model specification 175 - 3300 nm) spectrophotometer. Measurements were done in the wavelength range of 200 to 800 nm. Further, Raman spectra were obtained in the Raman shift range between 200 - 1500 cm^{-1} by Lab India make instrument. Laser beam of wavelength λ = 532 nm was used for the measurements.

FTIR absorption measurements

A few micrograms of each sample were mixed to a predetermined amount of pure KBr and thoroughly pulverized. The homogenous mixture was then formed into pellet form. The FTIR spectra of a pure KBr pellet was subtracted from the FTIR data of each sample to remove the moisture absorption effects. FTIR measurements were carried out by using FTIR Alpha-II instrument in the range of 500 - 4000 cm^{-1}, where different modes of vibration could be observed which gives the structural information of Nb_2O_5.

Results and Discussion

Structural analysis

XRD results are shown in figure 1 which gives the structural information. The most intense peak was obtained at 22.62°. The average crystallite sizes of the particles observed for sample A and sample B were ~23 nm and 18 nm, respectively. The Rietveld refinement (not shown here) showed that sample have orthorhombic crystalline phase (T-phase) with lattice parameters (a = 6.165 Å, b = 29.135 Å, and c = 3.914 Å) and match well with the literature reports (PDF cards No. 30-0873) for the T-Nb_2O_5 phase. It is clear that capping agents reduces the size of Nb_2O_5 NPs.

UV-Vis spectroscopy

Figure 2 and figure 3 depict the UV-Vis spectra of Nb_2O_5 (sample A and sample B) NPs. The spectra reveal information regarding nanomaterial excitation or inner band transitions. Values of bandgap (E_g) were calculated using linear regression of the absorption slope and extrapolation of the tangent to the energy as shown in the insets of figure 2 and figure 3. The Kubelka-Munk theory of diffuse reflectance was employed in the analysis to extract a function proportional to absorbance of the samples. Kubelka-Munk theory is effective for plotting

absorbance and getting band gap with the help of Tauc plot [7]. The energy-dependent absorption coefficient α can be expressed by equation 2 as per the Tauc method.

$$(\alpha h\nu)^{\frac{1}{\gamma}} = B\left(h\nu - E_g\right) \quad (2)$$

Where E_g is the energy band gap, ν is the photon's frequency, h is the Planck constant and B is a constant. The factor γ has values 1/2 or 2, this depends on the transfer type of electron, for the direct and indirect transition band gaps, respectively. The Kubelka-Munk function can be used in accordance with Kubelka-Munk's theory, to convert observed reflectance spectra into their corresponding absorption spectra.

$$F(R) = \frac{K}{S} = \frac{(1-R)^2}{2R} \quad (3)$$

Instead of α, Putting F(R) into equation 2 yields the form, where R is the reflectance, while S and K are the scattering and absorption coefficients, respectively [8, 9].

$$(F(R).h\nu)^{\frac{1}{\gamma}} = B\left(h\nu - E_g\right) \quad (4)$$

Band gaps of sample A and sample B were calculated as 3.22 and 3.19 eV, respectively. Figure 2 and figure 3 shows the graph between absorbance vs wavelength, in which maximum absorption was observed nearly at 276 nm. The λ_{max} values for both samples have been obtained as between 270 to 380 nm in the absorption spectra, which display a blue shift for the synthesized Nb_2O_5 NPs compared to their bulk counterpart. This blue shift can be caused by the size quantization effect in the prepared Nb_2O_5 NPs [6].

FTIR results

Figure 4a and 4b show the transmission FTIR spectra recorded on Nb_2O_5 NPs (Sample A and Sample B). We observed the bands between 4000 - 3600 cm^{-1} due to vibrations of -OH group of absorbed water. In sample A, this band appears at 3384 cm^{-1} and in sample B, the band appears at 3416 cm^{-1}. It is clear from the figures that the peak due to -OH was deep and broadened in sample B may be due to changed quantity of capping agent. Another stretching vibrational mode peaks appear in figure 4b at 2927 cm^{-1} and 2337 cm^{-1} which are almost flat in figure 4a. The peaks at 1627 cm^{-1} and 1628 cm^{-1} in figure 4a and 4b show the bending vibrations of absorbed water. The region between 1500 cm^{-1} to 500 cm^{-1} is known as fingerprint region. The bands in this region, at 1019 cm^{-1} appears sharply in sample A (shown in figure 4a) due to the stretching vibrations of C-O bond and in sample B this band is shifted to 1071 cm^{-1}. The bands at 953 and 878 cm^{-1} also show the stretching vibrations of C=O or O-O, while the bands at 738 and 539 cm^{-1} (figure 4a) show stretching vibrations of Nb-O-Nb and Nb=O. Similarly, the bands at 814, 719 and 609 cm^{-1} (figure 4b) are indications of Nb-O, Nb-O-Nb and Nb=O stretching vibrations. It is clear that the region between 3400 - 1800 cm^{-1} of sample A looks flat as compared to sample B and the vibrations of sample A in fingerprint region are more pronounced than sample B [10-12].

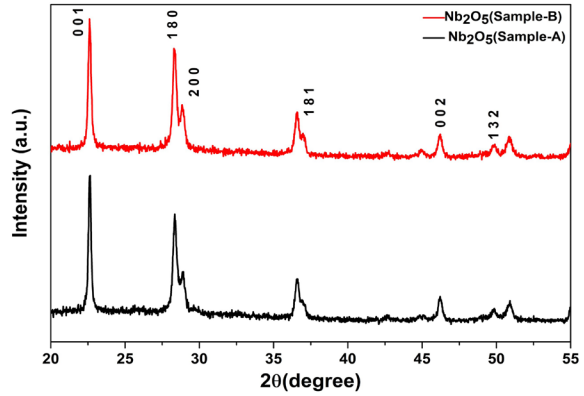

Figure 1: XRD pattern of Nb_2O_5 NPs.

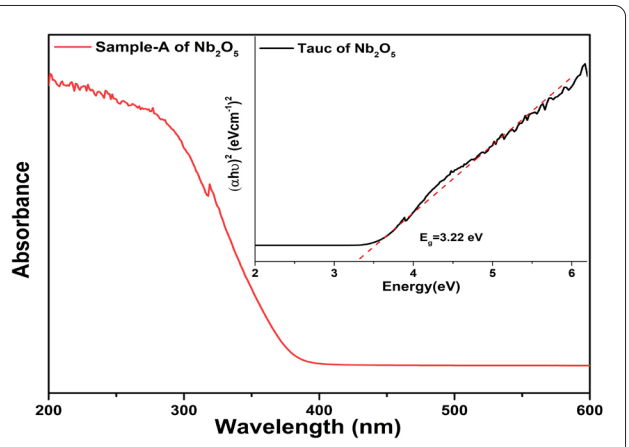

Figure 2: UV-Vis spectrum of sample A.

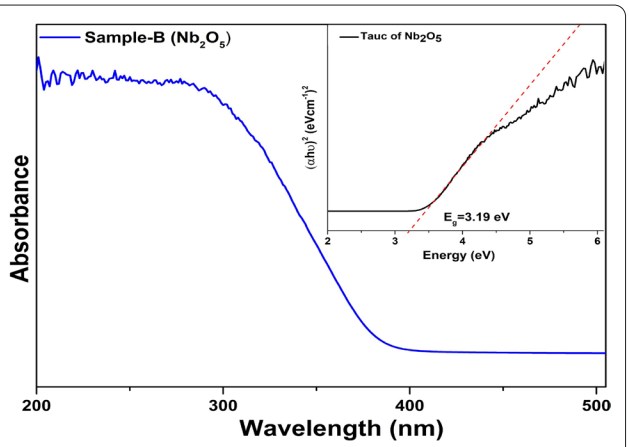

Figure 3: UV-Vis spectrum of sample B.

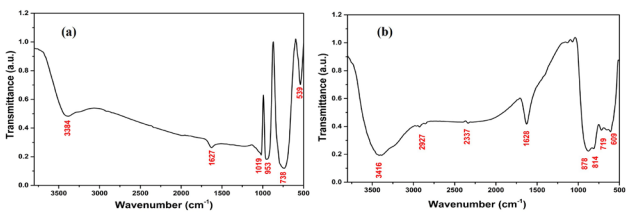

Figure 4: FTIR of Nb_2O_5 NPs **(a)** Sample A and **(b)** Sample B.

Raman spectroscopy

The vibrational characterization was carried out using Raman spectroscopy. Spectra were obtained in the Raman shift range of 200 - 1500 cm^{-1} for both samples as shown in figure 5a and 5b. The main element in the amorphous or polycrystalline phase of Nb_2O_5 is the NbO_6 octahedron. The NbO_6 octahedra in the crystal lattice vibrate in a variety of ways, resulting in different frequency areas that may be identified in the Raman spectrum of Nb_2O_5. The appearance of Raman active band at 351.8 cm^{-1} in sample A is not seen in sample B, which shows different Raman bands at 222.5 and 308 cm^{-1}, suggesting a modification in the vibrational properties. All these are NbO_6 octahedra bending modes of vibration [13, 14]. The sharp and intense peaks at 717 and 685 cm^{-1} indicate high crystallinity of the material and it is clear from figure 5a and 5b that sample B has sharper peak as compared to sample A. These bands/peaks are due to the symmetric or asymmetric stretching modes of Nb and O. The peak at 1061 cm^{-1} which almost disappeared in figure 5b gives indications of edge shared octahedra [15].

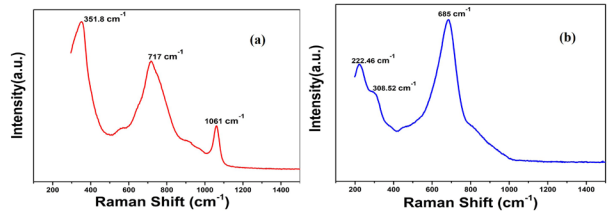

Figure 5: Raman spectra of Nb_2O_5 NPs **(a)** Sample A and **(b)** Sample B.

Conclusion

Successful synthesis of Nb_2O_5 NPs was achieved in the current work using chemical synthesis route. It was observed that PVP is a non-ionic polymer, and it is water soluble, so it plays a good role to control the agglomeration of Nb_2O_5 NPs by acting as a capping agent. The crystalline size was found to decrease as the quantity of PVP increased. The FTIR vibrations in the range 1000 - 600 cm^{-1} and Raman bands at their respective positions indicate the bending structure of Nb_2O_5. Difference in band gap values shows the effect of capping agent that modifies the average crystallite size as well. These observed results are very useful for making Nb_2O_5 NPs based modified electrode that can be taken up as a future work. These electrodes may be used to make electrochemical sensors for sensing environmental toxicity in water samples and they can also be used in gas sensor.

Acknowledgments

Authors would like to acknowledge Dr. Uday Deshpande, UGC-DAE CSR, Indore for sample characterization.

Conflict of Interest

None.

References

1. Singh J, Tripathi J, Sharma M, Valuskar A, Chandrawat GS, et al. 2020. Structural investigation and optical properties of silver nanoparticles synthesis by chemical method. *J Nano Electron Phys* 12(2): 02006.
2. Ding H, Song Z, Zhang H, Li X. 2020. Niobium-based oxide anodes toward fast and safe energy storage: a review. *Mater Today Nano* 11: 100082. https://doi.org/10.1016/j.mtnano.2020.100082
3. Vorokhta M, Khalakhan I, Vondráček M, Tomeček D, Marešová E, et al. 2018. Investigation of gas sensing mechanism of SnO_2 based chemiresistor using near ambient pressure XPS. *Surf Sci* 677: 284-290. https://doi.org/10.1016/j.susc.2018.08.003
4. Mavrou G, Galata S, Tsipas P, Sotiropoulos A, Panayiotatos Y, et al. 2008. Electrical properties of La_2O_3 and HfO_2/ La_2O_3 gate dielectrics for germanium metal-oxide-semiconductor devices. *J Appl Phys* 103(1): 014506. https://doi.org/10.1063/1.2827499
5. Marcondes LM, Maestri S, Sousa B, Gonçalves RR, Cassanjes FC, et al. 2018. High niobium oxide content in germanate glasses: thermal, structural, and optical properties. *J Am Ceram Soc* 101(1): 220-230. https://doi.org/10.1111/jace.15215
6. Hidde J, Guguschev C, Klimm D. 2019. Thermal analysis and crystal growth of doped Nb_2O_5. *J Cryst Growth* 509: 60-65. https://doi.org/10.1016/j.jcrysgro.2018.12.035
7. Lindberg JD, Snyder DG. 1973. Determination of the optical absorption coefficient of powdered materials whose particle size distribution and refractive indices are unknown. *Appl Opt* 12(3): 573-578. https://doi.org/10.1364/AO.12.000573
8. Makuła P, Pacia M, Macyk W. 2018. How to correctly determine the band gap energy of modified semiconductor photocatalysts based on UV-Vis spectra. *J Phys Chem Lett* 9(23): 6814-6817. https://doi.org/10.1021/acs.jpclett.8b02892
9. Rambadey OV, Kumar A, Sati A, Sagdeo PR. 2021. Exploring the interrelation between Urbach energy and dielectric constant in Hf-substituted $BaTiO_3$. *ACS Omega* 6(47): 32231-32238. https://doi.org/10.1021/acsomega.1c05057
10. Vosoughifar M. 2017. Preparation of nanocrystalline niobium pentoxide with different morphologies via a thermal decomposition route. *J Mater Sci Mater Electron* 28: 532-536. https://doi.org/10.1007/s10854-016-5555-5
11. Park H, Lee D, Song T. 2019. High capacity monoclinic Nb_2O_5 and semiconducting NbO_2 composite as high-power anode material for Li-ion batteries. *J Power Sources* 414: 377-382. https://doi.org/10.1016/j.jpowsour.2019.01.015
12. Anandhi S, Keerthika D, Edward M, Jaisankar V. 2020. Synthesis and characterization of niobium oxide nanoparticles, polyindole and Nb_2O_5/polyindole nanocomposite. *Asian J Chem* 32(3): 653-658.
13. Shafeeqa SR, Salimb ET, AbdulRazzaq MJ, Wahid MHA. 2022. Effect of different parameters on Raman scattering released from Nb_2O_5 nanostructures prepared via PLD technique. *Eng Technol J* 40(10): 1325-1333. https://doi.org/10.30684/etj.2022.134436.1238
14. Sotillo B, Ariza R, Fernández P, Solis J. 2022. Ultrafast-laser powder bed fusion of oxygen-deficient Nb_2O_5 ceramics with highly improved electrical properties. *Mater Des* 224: 111346. https://doi.org/10.1016/j.matdes.2022.111346
15. Raba AM, Bautista-Ruíz J, Joya MR. 2016. Synthesis and structural properties of niobium pentoxide powders: a comparative study of the growth process. *Mater Res* 19: 1381-1387. https://doi.org/10.1590/1980-5373-MR-2015-0733